

Pruning for Interpretable, Feature-Preserving Circuits in CNNs

Chris Hamblin* Talia Konkle George Alvarez
 chrishamblin@fas.harvard.edu tkonkle@fas.harvard.edu alvarez@wjh.harvard.edu
 Harvard University, Department of Psychology

Abstract

Deep convolutional neural networks are a powerful model class for a range of computer vision problems, but it is difficult to interpret the image filtering process they implement, given their sheer size. In this work, we introduce a method for extracting “feature-preserving circuits” from deep CNNs, leveraging methods from saliency-based neural network pruning. These circuits are modular sub-functions, embedded within the network, containing only a subset of convolutional kernels relevant to a target feature. We compare the efficacy of 3 saliency-criteria for extracting these sparse circuits. Further, we show how ‘sub-feature’ circuits can be extracted, that preserve a feature’s responses to particular images, dividing the feature into even sparser filtering processes. We also develop a tool for visualizing ‘circuit diagrams’, which render the entire image filtering process implemented by circuits in a parsable format.

1 Introduction

There is no doubt that modern deep learning techniques have dramatically changed the way engineers approach computer vision problems, replacing hand-engineered image processing algorithms with large neural networks trained end-to-end. While this has improved model performances on a range of tasks, it leaves the underlying algorithms opaque. As deep-learned models become ubiquitous for computer-vision applications, this poses a notable concern, sparking a general interest in neural network *interpretability*.

Work in neural network interpretability can be divided into two broad categories, that of data *representation*, and data *processing* Gilpin *et al.* (2019). Much of the interpretability work in computer vision concerns data representation, or *what* the network represents, in the conceptual sense. The focus on representation usually leads to methods for mapping network features back into pixel space, where the researcher can employ their own visual capacities to make inferences about the latent space of the network. Examples of such representational interpretability methods include viewing the output activation maps of a cnn filter Yosinski *et al.* (2015), the attention map in a visual transformer Caron *et al.* (2021), viewing dataset examples or feature visualizations Erhan *et al.* (2009); Olah *et al.* (2017) that maximally excite/inhibit a latent feature, or attribution methods Selvaraju *et al.* (2019); Zeiler & Fergus (2014); Sundararajan *et al.* (2017) that highlight pixel regions most responsible for a model’s response. Other work Zhou *et al.* (2018) ascribes semantic labels to latent features that align with the annotations in densely segmented image sets Zhou *et al.* (2017); Mottaghi *et al.* (2014); Bell *et al.* (2014); Chen *et al.* (2014); Cimpoi *et al.* (2014). Much less common are accounts of data processing, e.g. an interpretable sequence of computations that generate representations. So, while a researcher might be confident a feature in their model acts as, say, a brown fur detector, this is not necessarily coupled with a formal understanding of how a brown fur detector is built. In general, while it is often possible to trace how the first layer of features are

*email for correspondence. Code available at https://github.com/chrishamblin7/circuit_pruner

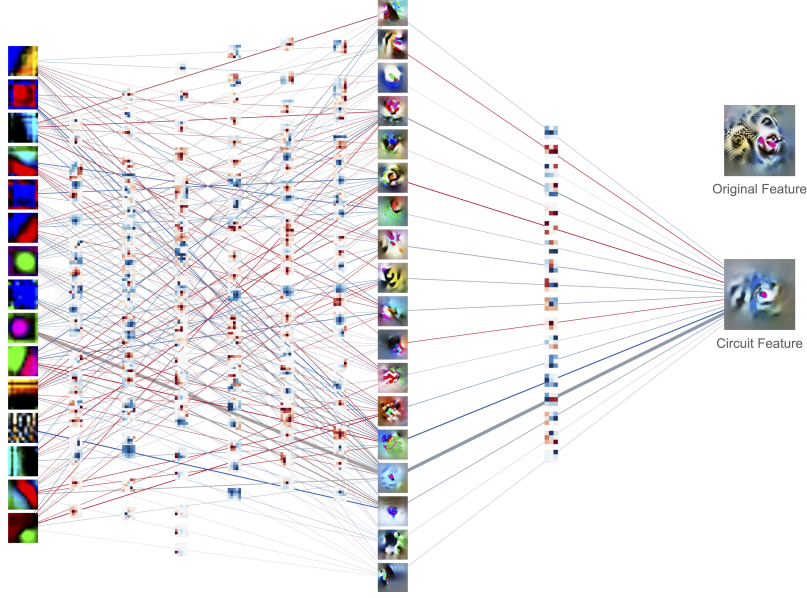


Figure 1: An *extended circuit diagram* of feature *conv3:56* in Alexnet. See section 4 for a full account.

constructed from weights over the input in a deep net, the computation graph becomes increasingly unwieldy when considering features in later layers.

The architectural constraint of convolutional neural networks allows for greater *data processing* interpretability than many other deep models. The kernel convolution operation not only reduces the number of parameters to contend with by replicating weights across space, but also constrains the function space learnable by the network to a familiar subspace. Kernel convolution operations are typical in hand-engineered image processing algorithms, where single kernels can enable filters for edge detection, sharpening, blurring, spatial frequency filtering, etc Nixon & Aguado (2012); Kanopoulos *et al.* (1988). Composing filters in a hierarchy enables the construction of more complex detectors, with each kernel acting as a spatial template for the arrangement of features from the previous layer. Cammarata *et al.* (2020) Cammarata *et al.* (2020) show that viewing feature visualizations in conjunction with the kernels connecting them provides strong visual intuition for how simple features are combined into complex ones. The authors describe many interesting ‘circuits’ they’ve discovered in InceptionV1 Szegedy *et al.* (2015), from early circuits encoding curves and basic shapes, to late-layer circuits encoding real-world objects. A prototypical circuit from their work shows how a car feature is constructed with three kernels spatially arranging features in the previous layer for windows, wheels, and car bodies Olah *et al.* (2020).

Circuits provide a promising framework for interpreting the image filtering processes latent in CNNs, and this work aims to bolster the approach by addressing two related issues. Firstly, when considering the aforementioned ‘car circuit’ composed of wheel and window features, the immediate questions arise, ‘But what then is the wheel circuit? What is the window circuit? I can’t fully grasp the car feature without grasping these constituent parts.’ As such, it would be useful to *extend* circuit diagrams backwards layer-wise towards the inputs, as diagrammed in Fig 1. Such a diagram runs the risk of being massive and unparsable, presenting our second issue; which kernels (edges) do we include in the diagram, and how do we avoid over-simplifying our target feature given our exclusions? This concern with over-simplification is also present in the original circuit work; diagramming the car feature with 3 kernels is certainly parsimonious, but ignoring the effects of the hundreds of other kernels in the original filter may result in a much degraded feature.

In the present work, we address these issues by re-purposing techniques from neural network pruning for *circuit extraction*. We’ll compare the efficacy of several saliency-based pruning methods for extracting sparse sub-networks that preserve a target feature’s responses to input images *without fine-tuning*. The differences in responses returned by such a circuit formalize the effect of an interpretability researcher *zooming in* (to use the term from Olah *et al.* (2020)), focusing on some computations while ignoring others, as is a pragmatic necessity. Further, our method allows the

researcher to zoom-in in a principled way, by identifying small subsets of computations that approximate the original feature when considered in isolation. In a follow-up set of experiments, we will show how our method can be used to extract *sub-feature* circuits, which preserve feature responses only to a target set of images, dividing complex features into component parts. Lastly, we will explain how sparse circuits can be visualized with our circuit diagramming tool (Fig 1).

2 Methods

2.1 Notation

This work concerns convolutional layers in deep neural networks. The l th convolutional layer takes a stack of *activation maps* as input, $\mathbf{A}^{l-1} \in \mathbb{R}^{C_{\text{in}} \times H_{\text{in}} \times W_{\text{in}}}$ and outputs the activation maps $\mathbf{A}^l \in \mathbb{R}^{C_{\text{out}} \times H_{\text{out}} \times W_{\text{out}}}$. The layer is composed of C_{out} *filters* (one for each output channel), each parameterized by weights $\mathbf{w}_{c_{\text{out}}}^l \in \mathbb{R}^{C_{\text{in}} \times K_h \times K_w}$ and bias $b_{c_{\text{out}}}^l \in \mathbb{R}$. Each filter transforms input activation maps to output maps by;

$$\mathbf{A}_{c_{\text{out}}}^l = \sum_{c_{\text{in}}=1}^{C_{\text{in}}} \mathbf{w}_{c_{\text{out}}, c_{\text{in}}}^l * \mathbf{A}_{c_{\text{in}}}^{l-1} + b_{c_{\text{out}}}^l, \quad (1)$$

where $*$ denotes the convolution. A filter is composed of C_{in} 2D *kernels* with weights $\mathbf{w}_{c_{\text{out}}, c_{\text{in}}}^l \in \mathbb{R}^{K_h \times K_w}$ which compute the kernel-wise activation map $\mathbf{A}_{c_{\text{out}}, c_{\text{in}}}^l \in \mathbb{R}^{H_{\text{out}} \times W_{\text{out}}}$, before the filter sums these maps element-wise and adds its bias. Individual activations in any activation map are denoted as $a_{c_{\text{out}}, c_{\text{in}}, h, w}^l$. A *feature* refers to the full function from pixel-space that returns a particular activation, denoted $\mathcal{F}(x) = a$. An activation map returns the same feature $H_{\text{out}} \times W_{\text{out}}$ times with respect to the *image patches* in each activation’s effective receptive field Le & Borji (2017); Araujo *et al.* (2019). For the pruning methods section, $\boldsymbol{\theta} = \{\theta_j\}_{j=1}^m$ refers to the flattened vector of all network parameters.

2.2 Problem Statement

We endeavor to simplify the data processing underlying a particular feature by removing parameters from the network, while minimally affecting the feature’s activations. We can formulate our *circuit pruning* problem similarly to conventional pruning; given a latent feature \mathcal{F} in a network and a set of input images (or image patches) $\mathcal{D} = \{\mathbf{x}_i\}_{i=1}^n$, we want to identify a subnetwork parameterized by $\bar{\boldsymbol{\theta}}$ under a sparsity constraint, such that the change in \mathcal{F} ’s responses to \mathcal{D} is minimized:

$$\begin{aligned} \underset{\bar{\boldsymbol{\theta}}}{\arg \min} \Delta \mathcal{F}(\bar{\boldsymbol{\theta}}, \boldsymbol{\theta}; \mathcal{D}) &:= \sum_{i=1}^n |\mathcal{F}(\boldsymbol{\theta}; \mathbf{x}_i) - \mathcal{F}(\bar{\boldsymbol{\theta}}; \mathbf{x}_i)| \\ \text{s.t.} \quad &\|\bar{\boldsymbol{\theta}}\|_0 \leq \kappa, \quad \bar{\theta}_j \in \{\theta_j, 0\} \quad \forall j \in \{1 \dots m\} \end{aligned} \quad (2)$$

$\bar{\boldsymbol{\theta}}$ corresponds to a sparse path of computations through the full network that generates an approximation of the target feature, with no more than κ parameters. The constraint that $\bar{\theta}_j \in \{\theta_j, 0\} \quad \forall j \in \{1 \dots m\}$ ensures that we cannot fine-tune the network, that circuits we extract are latent within the network *as is*.

As is typical with pruning problems, finding an optimal $\bar{\boldsymbol{\theta}}$ cannot be brute forced, as there exist $\binom{m}{\kappa}$ possible parameterizations. Fortunately, many saliency-based approaches to pruning have a similar problem statement to (eq 2) in that they endeavor to find a sparse $\bar{\boldsymbol{\theta}}$ that minimally changes the loss function \mathcal{L} of the original model. Such methods consider quickly-computable, parameter-wise *saliency criteria* $S(\theta_j)$ meant to approximate $|\Delta \mathcal{L}|$ induced by removing individual parameters. With a simple substitution of \mathcal{F} for \mathcal{L} , these saliency criteria should be well suited for our problem. We

can then replace (eq 2) with the simpler problem of identifying a parameterization $\bar{\theta}$ with maximal cumulative saliency;

$$\begin{aligned} \underset{\bar{\theta}}{\arg \max} S_{sum}(\bar{\theta}) &:= \sum_{j \in \text{supp}(\bar{\theta})} S(\theta_j) \\ \text{s.t. } \quad &\|\bar{\theta}\|_0 \leq \kappa, \quad \bar{\theta}_j \in \{\theta_j, 0\} \quad \forall j \in \{1 \dots m\} \end{aligned} \quad (3)$$

Where solving problem (eq 2) is hard, solving problem (eq 3) is easy, just choose parameters θ_j with the top- κ $S(\theta_j)$ for inclusion in $\bar{\theta}$.

In this work we test the efficacy of 3 saliency criteria from the literature on our circuit pruning problem, *SNIP* Lee *et al.* (2018); Mozer & Smolensky (1988), *FORCE* de Jorge *et al.* (2020), and *actgrad* Molchanov *et al.* (2019). These are all first order saliency criteria, utilizing gradients. While other methods exist that utilize the Hessian Cun *et al.* (1990); Hassibi *et al.* (1993); Wang *et al.* (2020), these are motivated by the observation that training a network with gradient descent should push $\frac{\partial \mathcal{L}}{\partial \theta}$ to 0, but this does not necessarily hold for $\frac{\partial \mathcal{F}}{\partial \theta}$.

2.3 Circuit SNIP

While the SNIP saliency criterion was originally introduced in Mozer & Smolensky (1988), Lee *et al.* (2018) Lee *et al.* (2018) demonstrated the criterion’s efficacy for *single-shot* pruning at initialization Wang *et al.* (2020); Verdenius *et al.* (2020); de Jorge *et al.* (2020), which utilizes no fine-tuning, making the criterion promising for our application. In SNIP, a binary mask $\mathbf{c} \in \{0, 1\}^m$ is inserted into the network, such that the new network is parameterized by $\mathbf{c} \odot \theta$, where \odot denotes the Hadamard product. In the original un-pruned network, $\mathbf{c} = \{1\}^m$. When $c_j = 0$, this is equivalent to parameter θ_j being pruned from the network. The authors reason the importance of parameter θ_j to be proportional to the effect on the loss were it to be removed, or equivalently $c_j = 0$:

$$\Delta \mathcal{L}_j(c_j; \mathcal{D}) = \mathcal{L}(c_j = 1; \mathcal{D}) - \mathcal{L}(c_j = 0; \mathcal{D}), \quad (4)$$

The authors’ *connection sensitivity* saliency criterion considers the gradient of \mathcal{L} with respect to c_j . $|\partial \mathcal{L} / \partial c_j|$ measures the sensitivity of \mathcal{L} to perturbations of c_j , which they regard as an approximation of the $|\Delta \mathcal{L}_j|$ induced by setting $c_j = 0$. Their criterion can be equivalently calculated as the magnitude of parameters multiplied by their gradients:

$$S_{snip}(\theta) := |\partial \mathcal{L} / \partial \mathbf{c}| = \left| \frac{\partial \mathcal{L}(\theta \odot \mathbf{c})}{\partial \mathbf{c}} \right|_{\mathbf{c}=\mathbf{1}} = \left| \frac{\partial \mathcal{L}}{\partial \theta} \odot \theta \right| \quad (5)$$

We are interested in identifying network parameters that will affect some target feature’s average response when removed, rather than the loss. We thus formulate the circuit SNIP saliency criterion with the simple \mathcal{F} for \mathcal{L} substitution proposed above:

$$S_{snip}(\theta; \mathcal{F}) := |\partial \mathcal{F} / \partial \mathbf{c}| = \left| \frac{\partial \mathcal{F}}{\partial \theta} \odot \theta \right| \quad (6)$$

2.4 Circuit Force

The above SNIP criterion considers the effects of removing parameters in isolation, where in actuality we are endeavoring to remove many parameters from the network. Removal of a particular θ_j may have a very different effect when the network is fully-intact versus removal when other parameters are also pruned. Suppose our sparse network is parameterized by $\bar{\theta}$, then $S_{snip}(\bar{\theta})$ will certainly be different than $S_{snip}(\theta)$, as the gradients passing through the network will be different. Motivated by this observation, de Jorge *et al.* (2020) de Jorge *et al.* (2020) (and similarly Verdenius *et al.* (2020)) developed the *FORCE* saliency criterion (foresight connection sensitivity), which attempts to identify important parameters for the resultant sparse network, despite the unfortunate circularity that this

sparse network is supposed to be identified *by way of* the saliency criterion. The author's make a subtle adjustment to the saliency-based pruning problem statement (eq 3);

$$\begin{aligned} \arg \max_{\bar{\theta}} S_{force_sum}(\bar{\theta}) &:= \sum_{j \in \text{supp}(\bar{\theta})} S_{snip}(\bar{\theta}_j) \\ \text{s.t. } \quad &\|\bar{\theta}\|_0 \leq \kappa, \quad \bar{\theta}_j \in \{\theta_j, 0\} \quad \forall j \in \{1 \dots m\}. \end{aligned} \quad (7)$$

They still endeavor to find a $\bar{\theta}$ with maximum cumulative saliency, but when parameter-wise saliency is measure in the pruned network, rather than the original network as in (eq 3).

Unfortunately (eq 7) is not trivial to solve as is (eq 3), but the authors reason an approximate solution can be obtained by iteratively masking an increasing number of parameters, recomputing $S_{snip}(\bar{\theta})$ at each step to get the next mask by way of (eq 3). Let's call the network parameterization after the first masking iteration $\bar{\theta}_1$, the second $\bar{\theta}_2$, up to the final iteration T with a parameterization at the desired sparsity $\bar{\theta}_T$. The motivating intuition for this iterative sparsification follows from the observation that the fewer parameters are masked from θ to obtain $\bar{\theta}_1$, the better the *gradient approximation* $\frac{\delta \mathcal{L}(\theta)}{\delta \theta} \approx \frac{\delta \mathcal{L}(\bar{\theta}_1)}{\delta \bar{\theta}_1}$ should hold, and we can use $S_{snip}(\theta)$ to approximate $S_{snip}(\bar{\theta}_1)$. This logic is inductive; $S_{snip}(\bar{\theta}_1)$ is a better approximation of $S_{snip}(\bar{\theta}_2)$ than $S_{snip}(\theta)$ (as there are fewer parameters masked between $\bar{\theta}_1$ and $\bar{\theta}_2$), $S_{snip}(\bar{\theta}_3)$ is better approximated by $S_{snip}(\bar{\theta}_2)$ than any of the previously computed scores, etc. In general $S(\theta_T)$ should be calculated with many iterations of S_{snip} , resulting in a small difference in the masks between iterations, to optimize (eq 7). In this work we implement *FORCE* with 10 iterations and the exponential decay scheduler from de Jorge *et al.* (2020), which were shown to be effective hyper-parameters in the original work (*appendix*). We note that while optimizing (eq 7) may lead to a *trainable* model parameterization with high connection sensitivity (as was the intention in the original work), we explicitly want to minimize $\Delta \mathcal{F}(\theta, \theta_T)$. With *FORCE*, at each iteration we are approximating *an approximation*, $\Delta \mathcal{F}(\theta_{i-1}, \theta_i)$. This could lead to divergence from \mathcal{F} , depending on the accuracy of the iterative approximations.

2.5 Circuits by Taylor Expansion

Another way of deriving an approximation for $\Delta \mathcal{L}$ given the removal of a parameter is by Taylor approximation. This approach was employed successfully by Molchanov et al (2019) Molchanov *et al.* (2019) for the pruning of convolutional filters. Their saliency criterion concerns the activations in the network, rather than the weights themselves. Suppose some particular activation a_j in the network were to be masked (set to 0), then the first order Taylor approximation of the loss is:

$$\mathcal{L}(a_i = 0) = \mathcal{L}(a_i) - \frac{\delta \mathcal{L}}{\delta a_i} a_i \quad (8)$$

As per usual, the authors wanted their salience criteria for an activation to approximate the magnitude of the change in loss when that activation is masked, which can be approximated with (eq 8);

$$S_{actgrad}(a_i) := |\mathcal{L}(a_i) - \mathcal{L}(a_i = 0)| = \left| \frac{\partial \mathcal{L}}{\partial a_i} \odot a_i \right| \quad (9)$$

As we did for SNIP, we can formulate an equivalent circuit saliency criterion by substituting \mathcal{L} with \mathcal{F} :

$$S_{actgrad}(\mathbf{a}; \mathcal{F}) := \left| \frac{\partial \mathcal{F}}{\partial \mathbf{a}} \odot \mathbf{a} \right| \quad (10)$$

Notice that this criterion is equivalent to S_{snip} , applied to activations as opposed to weights. Relatedly, the above taylor derivation is applicable to S_{snip} , and as such we denote this saliency criteria $S_{actgrad}$, rather than S_{taylor} as in Molchanov *et al.* (2019).

2.6 Structured Pruning of Kernels

It is sometimes practical to prune *structurally*, i.e. with respect to architecturally related groups of parameters. In the case of CNNs, this has typical meant pruning entire convolutional filters Molchanov *et al.* (2019); Luo *et al.* (2018); Luo & Wu (2017,?); Lin *et al.* (2019); Gamanayake *et al.* (2020); Luo & Wu (2020); He *et al.* (2018); Lin *et al.* (2018b); Ding *et al.* (2019), as this leads to models that are resource efficient when implemented with BLAS Blackford *et al.* (2002) libraries. Our goal is not resource efficiency, but rather to extract interpretable circuits from the model, and as such we will prune with respect to individual convolutional *kernels* Li *et al.* (2019); Zhu *et al.* (2021); Lin *et al.* (2018a); Mao *et al.* (2017). Kernels constitute the edges of our desired circuit diagrams (Fig 1), thus an extracted circuit with kernel sparsity should make for a maximally parsable diagram. To compute *kernel-wise* saliency scores, we simply average the saliency scores of the parameters within each kernel. For S_{snip} (and by extension S_{force}), this is the average saliency of each of the kernel’s weights. For $S_{actgrad}$, we average activations across the kernel-wise activation map. For a kernel k with weights \mathbf{w} and kernel-wise activation map \mathbf{A} ,

$$S_{snip}(k) := \frac{1}{K_w K_h} \sum_{w=1}^{K_w} \sum_{h=1}^{K_h} S_{snip}(w_{h,w}) \quad (11)$$

$$S_{actgrad}(k) := \frac{1}{H_{out} W_{out}} \sum_{w=1}^{W_{out}} \sum_{h=1}^{H_{out}} S_{actgrad}(a_{h,w}) \quad (12)$$

Pruning kernels to sparsity κ requires sorting the kernel-wise saliency scores and keeping the top- κ kernels, as before.

3 Experiments

All of the following experiments were conducted with a single NVIDIA *GeForce RTX 2080 Ti* GPU. All feature visualizations in this work were generated using the *Lucent* library Kiat (2020) (under an Apache License 2.0), a PyTorch implementation of *Lucid* Olah *et al.* (2017), using the default hyper-parameters.

3.1 Methods Comparison

To test our circuit pruning methods for feature preservation, we pruned circuits for features in an Imagenet Deng *et al.* (2009) trained Alexnet Krizhevsky *et al.* (2012). We tested two versions of this model, one trained in the typical manner, as is available through the Pytorch modelzoo Paszke *et al.* (2019), and one we trained with hierarchical group sparsity regularization Mitsuno *et al.* (2020). This regularization encourages groups of parameters (kernels and filters) towards zero magnitude during training (*appendix*). If we endeavor to find sparse circuits within a model, we reason it is useful to start with a model that already sparsely achieves the objective. We selected 20 random features from the last 3 of the model’s convolutional layers on which to test our methods. For each feature, we average the activations it returns to a subset of 2000 random images from Imagenet (2 images per category). This is the value for \mathcal{F} we use to compute kernel-wise saliency scores for each pruning method. As a baseline method, we additionally compute a *magnitude* kernel-wise saliency score, equal to the average magnitude of each weight in the kernel;

$$S_{magnitude}(k) := \frac{1}{K_w K_h} \sum_{w=1}^{K_w} \sum_{h=1}^{K_h} |w_{h,w}| \quad (13)$$

Using these saliency scores, we then extracted circuits at 13 sparsities, preserving 99%-1% of the *relevant* kernels with highest saliency. By *relevant*, we mean kernels that could possibly influence the target feature’s activations. These include all the kernels in the preceding layers and those kernels that belong to the feature’s filter itself, but no other kernels from that filter’s layer or later layers. For each of these extracted circuits, we computed the absolute value of the Pearson correlation between the original, un-pruned features’ activations to the 2000 images and the corresponding circuit features’

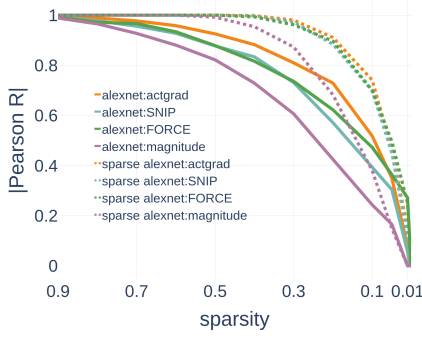


Figure 2: methods comparison.

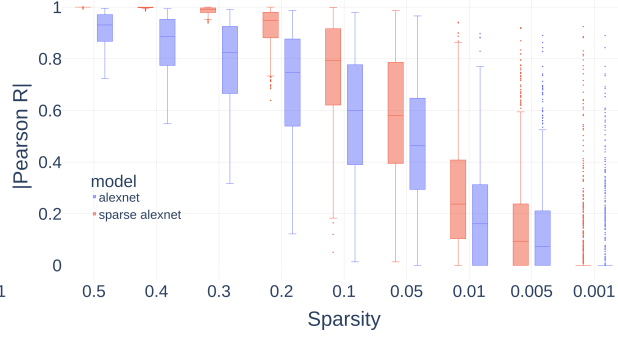


Figure 3: distributions of circuit/model feature correlations

activations. This metric measures the linearity of the relationship between the circuit feature and the original feature.

Fig 2 shows how well feature activations were preserved ($|$ Pearson’s $R|$), as a function of circuit sparsity, with separate lines for the three pruning methods, as well as the magnitude baseline method. The results show that *actgrad* is generally most effective for the Alexnet model, while *actgrad*, *SNIP* and *FORCE* perform similarly on the regularized Alexnet. *FORCE* shows a slight improvement with respect to the other metrics at the highest sparsities measured (though this effect is minimal, with a higher correlation of only $\Delta R \approx .08$). The results in de Jorge *et al.* (2020) showed *FORCE* is most effective in the high sparsity regime, and our results converge with this finding. Overall, all methods are able to extract sparse feature-preserving circuits well, outperforming the baseline magnitude saliency criterion.

These circuit extraction experiments also show that features in Alexnet are not homogenously sparse. Some features can maintain a high correlation with the full-model feature counterpart, even at extreme sparsities, while other features degrade quickly as more kernels are pruned. To get the full picture of the distribution of feature sparsities, we moved beyond the 60 features tested for methods comparison and next extracted circuits for every feature in the last 3 convolutional layers of Alexnet (896 features), using the *actgrad* method. We did not test all these features in the previous methods comparison experiment due to the long compute times for the *FORCE* method. Fig 3 shows these distributions of correlations for both models. Nearly all features tested are preserved (Pearson’s $R > .99$) at sparsities up to 50% in the regularized model. At higher sparsities ($\geq 20\%$) there is increasingly high variance in the correlations across features, but individual features can be identified that are well preserved at even the highest sparsity tested (.1% of relevant kernels kept).

3.2 Sub-Feature Circuits

The circuits we’ve extracted so far attempt to capture features as a whole, maintaining their responses to a broad sample of image patch inputs, but it may be useful for an interpretability researcher to extract *sub-feature* circuits, which preserve responses to a targeted selection of image patches. We are motivated here by the observation of *poly-semantic* Mu & Andreas (2020); Olah *et al.* (2017, 2020); Fong & Vedaldi (2018) features in CNNs, which respond selectively and highly to seemingly disparate semantic categories. Poly-semantic features may be composed of multiple, separable circuits with their own constituent kernels, with each circuit responsible for detecting only one of the semantic categories. The *general* circuit for a poly-semantic feature would then be the union of these category-wise circuits. In this case, an interpretability researcher should study these sub-feature circuits independently, as they constitute distinct image filtering processes. These sub-feature circuits would have the additional benefit of being ostensibly sparser than the general circuit for a feature.

To identify candidate poly-semantic features for our *sub-feature* extraction experiments, we took a data-driven approach. For each feature \mathcal{F}_j^l in the regularized Alexnet convolutional layers, we identified the top 300 individual activations it produced in response to the ImageNet training set, under the constraint that no two activations belong to the same activation map (are responses to different parts of the same image). Let $\mathbf{a}_j^l = \{a_{j,i}\}_{i=1}^{300}$ refer to these activations, and $\mathcal{D}_j^l = \{\mathbf{x}_{j,i}^l\}_{i=1}^{300}$ refer to

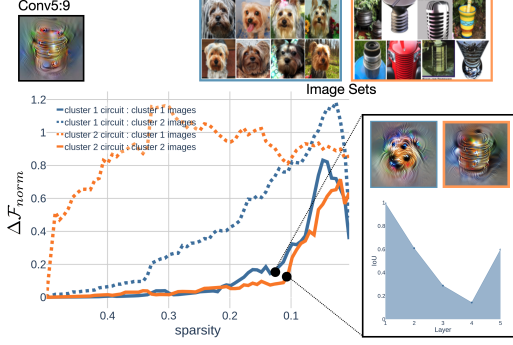


Figure 4: terrier/metal sub-feature circuits from clusters

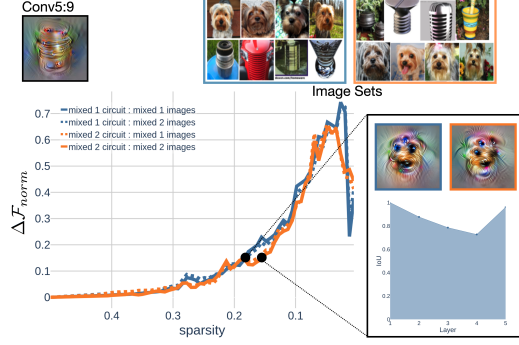


Figure 5: sub-feature circuits from mixed cluster

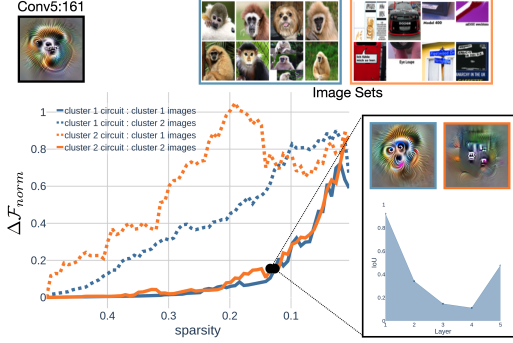


Figure 6: monkey/text sub-feature circuits

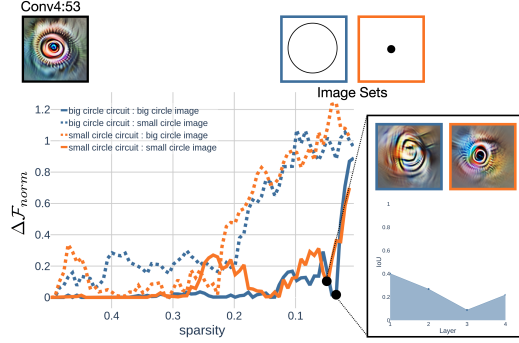


Figure 7: large/small circle sub-feature circuits

the corresponding image patches in each activation’s effective receptive field. We then consider layer l ’s population response to \mathcal{D}_j^l , a set of 300 activation vectors \mathcal{P}_j^l :

$$\mathcal{P}_j^l := \{p_{j,i}^l\}_{i=1}^{300} := \{\{\mathcal{F}_h^l(\mathbf{x}_{j,i}^l)\}_{h=1}^{C_{\text{out}}}\}_{i=1}^{300} \quad (14)$$

We reason that for a candidate poly-semantic feature \mathcal{F}_j^l , the set \mathcal{P}_j^l should be clusterable. This would suggest \mathcal{D}_j^l is represented as distinct groups in layer l ’s representation space, while the supposed poly-semantic feature \mathcal{F}_j^l makes no such distinction, as its activations \mathbf{a}_j^l are all very high, given our selection criteria for \mathbf{a}_j^l .

We used HDBScan clustering McInnes *et al.* (2017) to search for features with clusterable \mathcal{P}_j^l (under a BSD 3-Clause license). HDBScan works well in high-dimensions and requires only a minimum cluster size as its hyperparameter (we used 10). It will return anywhere from 0 to 30 clusters (300/10), allowing us to ignore filters that don’t show good clustering, and dissect other filters with respect to potentially many semantic groups (although in practice this approach rarely returned more than 2 clusters) (*appendix*).

Fig 4 shows the results of a pruning experiment on feature *Conv5:9* in regularized Alexnet. Our clustering analysis revealed this as a candidate poly-semantic filter, returning two distinct clusters, \mathcal{P}_1 and \mathcal{P}_2 . Qualitatively, the image patches corresponding to \mathcal{P}_1 and \mathcal{P}_2 (\mathcal{D}_1 and \mathcal{D}_2) look distinct, with one cluster corresponding to terrier faces, and the other corresponding to metal cylinders with horizontal lines, as can be seen in the sample of image patches in the top right of Fig 4. Next, we extracted different circuits for *Conv5:9*, which were intended to preserve *Conv5:9*’s responses to either \mathcal{D}_1 or \mathcal{D}_2 , using saliency scores $\mathcal{S}_{\text{actgrad}}(\mathbf{k}; \mathcal{F}; \mathcal{D}_1)$ and $\mathcal{S}_{\text{actgrad}}(\mathbf{k}; \mathcal{F}; \mathcal{D}_2)$. Rather than prune circuits from the full model, we start pruning from the *general circuit*, extracted in the previous experiment (sec 3.1), at 50% sparsity. This general circuit shows a very high correlation to the original filter’s activations ($>.999$ Pearson R). We extract the sub-filter circuits at 70 linearly spaced sparsities, preserving 49.99%-5% of the relevant kernels in the original model. The line plot in Fig 4 shows how these sub-filter circuits’ activations deviate from the general circuit’s activations as a

function of sparsity. The Y-axis shows a normalized measure of this deviation. For a sub-feature circuit parameterized by $\bar{\theta}$ and the general circuit by θ_{gen} :

$$\Delta\mathcal{F}_{norm}(\theta_{gen}, \bar{\theta}; \mathcal{D}) := \frac{\Delta\mathcal{F}(\theta_{gen}, \bar{\theta}; \mathcal{D})}{\frac{1}{n} \sum_{i=1}^n \mathcal{F}(\theta_{gen}; \mathbf{x}_i)} \quad (15)$$

With this metric, we can see how the sub-circuit’s activations deviate from the general circuit’s activations as a proportion of the general circuit’s activation magnitude. The solid lines show how the activations the circuit was meant to preserve deviate from the respective general circuit activations. Overall, we were able to extract sub-feature preserving circuits to high levels of sparsity.

Critically, we next examined how well these sub-feature circuits responded to the other cluster’s image patches (dotted lines). If the circuits act as distinct feature detectors, these responses should be far less preserved. The dotted lines in this plot clearly deviate at lower sparsities than the solid lines; we’ve identified circuits that preserve *Conv5:9* responses to only terriers but not metal cylinders, and visa-versa. To quantify the extent to which these specific sub-feature circuits involve different computations, we computed the intersection over union (IoU) of the sets of kernels belonging to each circuit. We compare the circuits at the last sparsity for which our $\Delta\mathcal{F}_{norm}$ remains below .15 for each circuit’s target activations. This intersection over union is shown as a function of layer depth in the bottom-right of Fig 4. It seems the two sub-feature circuits utilize the same layer 1 computations (gabors, center-surround filters etc.) but deviate from one another in subsequent layers. We also render feature visualizations for these extracted circuits, shown above the IoU plot. These show a clear distinction between the sub-feature circuits as well. Fig 6 shows the same analyses again, but for feature *conv5:161*, which is poly-semantic across monkey faces and written text.

As a control analysis, we extracted two new sub-feature circuits, this time with respect to a random 50/50 split of image patches from \mathcal{D}_1 and \mathcal{D}_2 . We hypothesized that these sub-feature circuits would not be separable. The results are shown in Fig 5 and confirm our hypothesis, indicated by the overlap between the solid and dashed lines, and the high IoU plot across the layers. Thus, for this feature, while separable sub-feature circuits exist for processing terrier faces and metal cylinders, they do not exist for any arbitrary set of images.

Finally, to test whether separable sub-feature circuits could be extracted without utilizing our clustering procedure, we attempted to *split* feature *Conv4:53* in a hypothesis-driven way. The top 300 highest activating image patches for *Conv4:53* show cocentric circles (*appendix*), and we hypothesized there may be separable circuits responsible for the feature’s response to large circles versus small circles, resulting in a scale-invariant circle detector. We attempt to isolate these circuits by extracting with respect to the two simple images in the top right of Fig 7, fit to the effective receptive field of *Conv4:53*. The pattern of data in Fig 7 reveals that this feature can indeed be split into separable circuits with respect to these images.

4 Extended Circuit Diagrams

Circuit pruning allows us to extract sparse sub-networks from a CNN that preserve the responses of targeted features. This reduces the size of features’ computation graphs, and allows for detailed inspection of how rich features are built. To facilitate this inspection, we have developed a tool for *extended circuit diagrams*. Fig 1 shows an extended circuit diagram for *conv3:56*, a feature that can be preserved at high sparsities according to our pruning experiments (sec 3.1). Following Olah et al (2020) Olah *et al.* (2020), edges in this diagram represent convolution with a 2D kernel, and vertices represent filters. Edge lines are colored based on the inhibition/excitation of their corresponding kernel (red for excitation, blue for inhibition, and gray for a mixture). The width of each edge line is proportional to the *actgrad* saliency score it received when pruning the circuit. Feature visualizations are displayed over their corresponding vertex, rendered with respect to the circuit, *not the original model* (unlike Olah *et al.* (2020)). This ensures the visualization is representative of the filtering operations displayed in the diagram. Additionally, our sparse circuit extraction allows for rendering of the *entire* circuit graph, with kernels/edges all the way back to the first convolutional layer (also unlike Olah *et al.* (2020)). We visualize the first layer’s features directly, by rendering the weights of each filter’s 3 kernels as the visualization’s 3 color channels.

Regarding Fig 1, where feature *conv3:56* had 12864 kernels preceding kernels in the original model, we’ve extracted a feature approximating circuit with only 210 kernels. Even at this high sparsity, Fig 1 is still a complex graph that’s difficult to parse as a static image. To remedy this, our full circuit diagramming tool comes equipped with a point-click GUI that allows the user to isolate individual vertices in the graph, with their incoming and outgoing edges. (*appendix*).

5 Conclusion & Future Work

In this work, we repurpose 3 saliency-based pruning methods for the extraction of feature preserving *circuits*. We compare the efficacy of these methods, finding they are similarly effective, and better than magnitude-based pruning. We then demonstrate how sparse circuits can be extracted that preserve features’ responses to only a selection of images. These extracted circuits constitute sparse image-filtering algorithms, which can be analyzed with our circuit diagramming tool. We’ve limited the current work to analyses of Alexnet, as our circuit diagramming tool does not currently support architectures with branching or skip connections. In the future we will extend this work to other CNN models. Additionally, our current experiments in ‘sub-filter’ pruning are largely hypothesis-driven, in the future we would like to develop data-driven methods for identifying separable sub-filter circuits in a network.

References

- Araujo, André, Norris, Wade, & Sim, Jack. 2019. Computing Receptive Fields of Convolutional Neural Networks. *Distill*. <https://distill.pub/2019/computing-receptive-fields>.
- Bell, Sean, Bala, Kavita, & Snavely, Noah. 2014. Intrinsic images in the wild. *ACM Transactions on Graphics (TOG)*, **33**(4), 1–12.
- Blackford, L Susan, Petitet, Antoine, Pozo, Roldan, Remington, Karin, Whaley, R Clint, Demmel, James, Dongarra, Jack, Duff, Iain, Hammarling, Sven, Henry, Greg, *et al.* 2002. An updated set of basic linear algebra subprograms (BLAS). *ACM Transactions on Mathematical Software*, **28**(2), 135–151.
- Cammarata, Nick, Carter, Shan, Goh, Gabel, Olah, Chris, Petrov, Michael, Schubert, Ludwig, Voss, Chelsea, Egan, Ben, & Lim, Swee Kiat. 2020. Thread: Circuits. *Distill*. <https://distill.pub/2020/circuits>.
- Caron, Mathilde, Touvron, Hugo, Misra, Ishan, Jégou, Hervé, Mairal, Julien, Bojanowski, Piotr, & Joulin, Armand. 2021. Emerging properties in self-supervised vision transformers. *Pages 9650–9660 of: Proceedings of the IEEE/CVF International Conference on Computer Vision*.
- Chen, Xianjie, Mottaghi, Roozbeh, Liu, Xiaobai, Fidler, Sanja, Urtasun, Raquel, & Yuille, Alan. 2014. Detect what you can: Detecting and representing objects using holistic models and body parts. *Pages 1971–1978 of: Proceedings of the IEEE conference on computer vision and pattern recognition*.
- Cimpoi, Mircea, Maji, Subhansu, Kokkinos, Iasonas, Mohamed, Sammy, & Vedaldi, Andrea. 2014. Describing textures in the wild. *Pages 3606–3613 of: Proceedings of the IEEE conference on computer vision and pattern recognition*.
- Cun, Yann Le, Denker, John S., & Solla, Sara A. 1990. Optimal Brain Damage. *Pages 598–605 of: Advances in Neural Information Processing Systems*. Morgan Kaufmann.
- de Jorge, Pau, Sanyal, Amartya, Behl, Harkirat, Torr, Philip, Rogez, Grégory, & Dokania, Puneet K. 2020. Progressive Skeletonization: Trimming more fat from a network at initialization. *In: International Conference on Learning Representations*.
- Deng, J., Dong, W., Socher, R., Li, L.-J., Li, K., & Fei-Fei, L. 2009. ImageNet: A Large-Scale Hierarchical Image Database. *In: CVPR09*.
- der Maaten, Laurens Van, & Hinton, Geoffrey. 2008. Visualizing data using t-SNE. *Journal of machine learning research*, **9**(11).

- Ding, Xiaohan, Ding, Guiguang, Guo, Yuchen, Han, Jungong, & Yan, Chenggang. 2019. Approximated oracle filter pruning for destructive cnn width optimization. *Pages 1607–1616 of: International Conference on Machine Learning*. PMLR.
- Erhan, Dumitru, Bengio, Yoshua, Courville, Aaron, & Vincent, Pascal. 2009. Visualizing Higher-Layer Features of a Deep Network. *Technical Report, Université de Montréal*, 01.
- Fong, Ruth, & Vedaldi, Andrea. 2018. Net2vec: Quantifying and explaining how concepts are encoded by filters in deep neural networks. *Pages 8730–8738 of: Proceedings of the IEEE conference on computer vision and pattern recognition*.
- Gamanayake, Chinthaka, Jayasinghe, Lahiru, Ng, Benny Kai Kiat, & Yuen, Chau. 2020. Cluster pruning: An efficient filter pruning method for edge ai vision applications. *IEEE Journal of Selected Topics in Signal Processing*, **14**(4), 802–816.
- Gilpin, Leilani H., Bau, David, Yuan, Ben Z., Bajwa, Ayesha, Specter, Michael, & Kagal, Lalana. 2019. Explaining Explanations: An Overview of Interpretability of Machine Learning. *International Conference on Data Science and Advanced Analytics*.
- Hassibi, Babak, Stork, David G, & Wolff, Gregory J. 1993. Optimal brain surgeon and general network pruning. *Pages 293–299 of: IEEE international conference on neural networks*. IEEE.
- He, Yang, Kang, Guoliang, Dong, Xuanyi, Fu, Yanwei, & Yang, Yi. 2018. Soft filter pruning for accelerating deep convolutional neural networks. *arXiv preprint arXiv:1808.06866*.
- Kanopoulos, Nick, Vasanthavada, Nagesh, & Baker, Robert. 1988. Design of an image edge detection filter using the Sobel operator. *IEEE Journal of solid-state circuits*, **23**(2), 358–367.
- Kiat, Lim Swee. 2020. *Lucent*. <https://github.com/greentfrapp/lucent>.
- Krizhevsky, Alex, Sutskever, Ilya, & Hinton, Geoffrey. 2012. ImageNet Classification with Deep Convolutional Neural Networks. *Neural Information Processing Systems*, **25**(01).
- Le, Hung, & Borji, Ali. 2017. What are the Receptive, Effective Receptive, and Projective Fields of Neurons in Convolutional Neural Networks? *CoRR*, **abs/1705.07049**.
- Lee, Namhoon, Ajanthan, Thalaiyasingam, & Torr, Philip. 2018. SNIP: SINGLE-SHOT NETWORK PRUNING BASED ON CONNECTION SENSITIVITY. *In: International Conference on Learning Representations*.
- Li, Yuchao, Lin, Shaohui, Zhang, Baochang, Liu, Jianzhuang, Doermann, David, Wu, Yongjian, Huang, Feiyue, & Ji, Rongrong. 2019 (June). Exploiting Kernel Sparsity and Entropy for Interpretable CNN Compression. *In: Proceedings of the IEEE/CVF Conference on Computer Vision and Pattern Recognition (CVPR)*.
- Lin, Chen, Zhong, Zhao, Wei, Wu, & Yan, Junjie. 2018a. Synaptic strength for convolutional neural network. *Advances in Neural Information Processing Systems*, **31**.
- Lin, Shaohui, Ji, Rongrong, Li, Yuchao, Wu, Yongjian, Huang, Feiyue, & Zhang, Baochang. 2018b. Accelerating Convolutional Networks via Global & Dynamic Filter Pruning. *Page 8 of: IJCAI*, vol. 2.
- Lin, Shaohui, Ji, Rongrong, Yan, Chenqian, Zhang, Baochang, Cao, Liujuan, Ye, Qixiang, Huang, Feiyue, & Doermann, David. 2019. Towards optimal structured cnn pruning via generative adversarial learning. *Pages 2790–2799 of: Proceedings of the IEEE/CVF Conference on Computer Vision and Pattern Recognition*.
- Luo, Jian-Hao, & Wu, Jianxin. 2017. An entropy-based pruning method for cnn compression. *arXiv preprint arXiv:1706.05791*.
- Luo, Jian-Hao, & Wu, Jianxin. 2020. Autopruner: An end-to-end trainable filter pruning method for efficient deep model inference. *Pattern Recognition*, **107**, 107461.

- Luo, Jian-Hao, Zhang, Hao, Zhou, Hong-Yu, Xie, Chen-Wei, Wu, Jianxin, & Lin, Weiyao. 2018. Thinet: pruning cnn filters for a thinner net. *IEEE transactions on pattern analysis and machine intelligence*, **41**(10), 2525–2538.
- Mao, Huizi, Han, Song, Pool, Jeff, Li, Wenshuo, Liu, Xingyu, Wang, Yu, & Dally, William J. 2017. Exploring the regularity of sparse structure in convolutional neural networks. *arXiv preprint arXiv:1705.08922*.
- McInnes, Leland, Healy, John, & Astels, Steve. 2017. hdbscan: Hierarchical density based clustering. *Journal of Open Source Software*, **2**(11), 205.
- Mitsuno, Kakeru, Miyao, Junichi, & Kurita, Takio. 2020 (07). Hierarchical Group Sparse Regularization for Deep Convolutional Neural Networks.
- Molchanov, P, Tyree, S, Karras, T, Aila, T, & Kautz, J. 2019. Pruning convolutional neural networks for resource efficient inference. In: *5th International Conference on Learning Representations, ICLR 2017-Conference Track Proceedings*.
- Mottaghi, Roozbeh, Chen, Xianjie, Liu, Xiaobai, Cho, Nam-Gyu, Lee, Seong-Whan, Fidler, Sanja, Urtasun, Raquel, & Yuille, Alan. 2014. The role of context for object detection and semantic segmentation in the wild. *Pages 891–898 of: Proceedings of the IEEE conference on computer vision and pattern recognition*.
- Mozer, Michael C, & Smolensky, Paul. 1988. Skeletonization: A Technique for Trimming the Fat from a Network via Relevance Assessment. In: Touretzky, D. (ed), *Advances in Neural Information Processing Systems*, vol. 1. Morgan-Kaufmann.
- Mu, Jesse, & Andreas, Jacob. 2020. Compositional explanations of neurons. *Advances in Neural Information Processing Systems*, **33**, 17153–17163.
- Nixon, Mark, & Aguado, Alberto S. 2012. *Feature Extraction & Image Processing for Computer Vision, Third Edition*. 3rd edn. USA: Academic Press, Inc.
- Olah, Chris, Mordvintsev, Alexander, & Schubert, Ludwig. 2017. Feature Visualization. *Distill*. <https://distill.pub/2017/feature-visualization>.
- Olah, Chris, Cammarata, Nick, Schubert, Ludwig, Goh, Gabriel, Petrov, Michael, & Carter, Shan. 2020. Zoom In: An Introduction to Circuits. *Distill*. <https://distill.pub/2020/circuits/zoom-in>.
- Paszke, Adam, Gross, Sam, Massa, Francisco, Lerer, Adam, Bradbury, James, Chanan, Gregory, Killeen, Trevor, Lin, Zeming, Gimelshein, Natalia, Antiga, Luca, Desmaison, Alban, Kopf, Andreas, Yang, Edward, DeVito, Zachary, Raison, Martin, Tejani, Alykhan, Chilamkurthy, Sasank, Steiner, Benoit, Fang, Lu, Bai, Junjie, & Chintala, Soumith. 2019. PyTorch: An Imperative Style, High-Performance Deep Learning Library. *Pages 8024–8035 of: Wallach, H., Larochelle, H., Beygelzimer, A., d'Alché-Buc, F., Fox, E., & Garnett, R. (eds), Advances in Neural Information Processing Systems 32*. Curran Associates, Inc.
- Selvaraju, Ramprasaath R., Das, Abhishek, Vedantam, Ramakrishna, Cogswell, Michael, Parikh, Devi, & Batra, Dhruv. 2019. Grad-CAM: Why did you say that? Visual Explanations from Deep Networks via Gradient-based Localization. *IJCV*, **abs/1610.02391**.
- Sundararajan, Mukund, Taly, Ankur, & Yan, Qiqi. 2017. Axiomatic attribution for deep networks. *Pages 3319–3328 of: International conference on machine learning*. PMLR.
- Szegedy, Christian, Liu, Wei, Jia, Yangqing, Sermanet, Pierre, Reed, Scott, Anguelov, Dragomir, Erhan, Dumitru, Vanhoucke, Vincent, & Rabinovich, Andrew. 2015. Going deeper with convolutions. *Pages 1–9 of: Proceedings of the IEEE conference on computer vision and pattern recognition*.
- Verdenius, Stijn, Stol, Maarten, & Forré, Patrick. 2020. Pruning via Iterative Ranking of Sensitivity Statistics. *CoRR*, **abs/2006.00896**.
- Wang, Chaoqi, Zhang, Guodong, & Grosse, Roger. 2020. Picking Winning Tickets Before Training by Preserving Gradient Flow. In: *International Conference on Learning Representations*.

Yosinski, Jason, Clune, Jeff, Nguyen, Anh Mai, Fuchs, Thomas J., & Lipson, Hod. 2015. Understanding Neural Networks Through Deep Visualization. *ICML*, **abs/1506.06579**.

Zeiler, Matthew D, & Fergus, Rob. 2014. Visualizing and understanding convolutional networks. *Pages 818–833 of: European conference on computer vision*. Springer.

Zhou, Bolei, Zhao, Hang, Puig, Xavier, Fidler, Sanja, Barriuso, Adela, & Torralba, Antonio. 2017. Scene parsing through ade20k dataset. *Pages 633–641 of: Proceedings of the IEEE conference on computer vision and pattern recognition*.

Zhou, Bolei, Bau, David, Oliva, Aude, & Torralba, Antonio. 2018. Interpreting deep visual representations via network dissection. *IEEE transactions on pattern analysis and machine intelligence*, **41**(9), 2131–2145.

Zhu, Jihong, Zhao, Yang, & Pei, Jihong. 2021. Progressive Kernel Pruning Based on the Information Mapping Sparse Index for CNN Compression. *IEEE Access*, **9**, 10974–10987.

6 Appendix

6.1 Code

Code for this project is available at https://github.com/chrishamblin7/circuit_pruner

6.2 Circuit Disconnect

At high sparsities a pruned circuit can become *disconnected* from its target feature, meaning there no longer exists a connected path of kernel convolution operations from the input to the target feature. We found from our experiments pruning many circuits with the *actgrad* criterion on regularized Alexnet, this happened only at the highest sparsities tested, .01, .005, and .001, with likelihoods of disconnection .057, .298, and .807 respectively. For the purposes of our reported Pearson R in the first experiments, we defined a disconnected circuit to have a Pearson R of 0.

Even when a circuit is not fully disconnected, it may still contain *dead-end* latent kernels/filters, for which there is no path forward to the target feature or backward to the input. Removing these *dead-end* kernels results in a sparser, yet functionally equivalent circuit. We call the sparsity of a circuit with its dead-ends removed *effective sparsity*. Fig 8 shows the relationship between circuit sparsity and effective sparsity for all *actgrad* circuits extracted from the regularized model, on a log/log scale. Each point represents a circuit, and the line represents equivalence between the sparsity measures (no dead-ends).

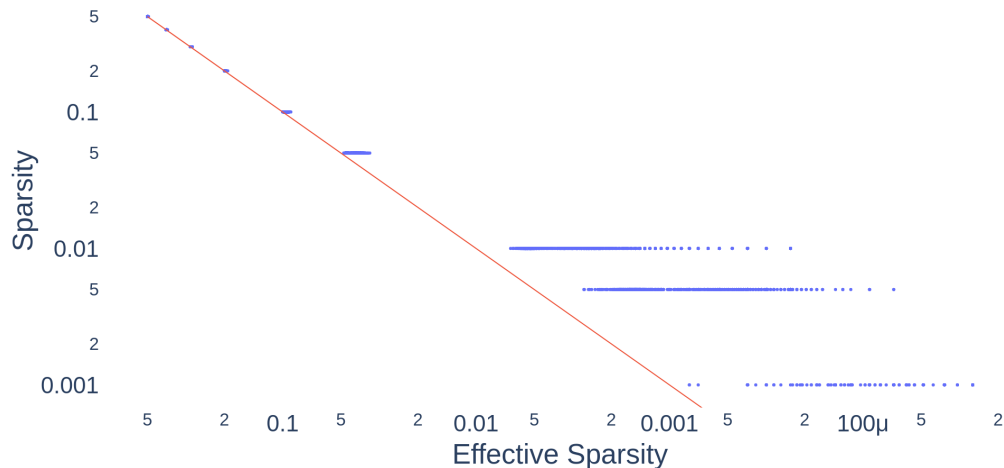


Figure 8: Sparsity versus effective sparsity of circuits

Finally, when extracting sub-networks for circuit diagrams, one must reconcile filters' *biases*. Suppose all of a filter's kernels have been pruned from a circuit, we wouldn't want to display such a filter (vertex) in the circuit diagram, but if we simply mask kernels to define the circuit's function, the filter *still* has an effect, as its bias remains. Thus, for circuits displayed as circuit diagrams, if a latent filter has all its kernels masked, we remove the entire filter, bias included. We call circuits with biases *masked* and circuits without biases *pruned*. This bias removal may have an effect on the circuit's feature preservation, thus in Fig 9 we compare the difference in Pearson R between *masked* and *pruned* circuits (pruned R - masked R), plotted as a function of effective sparsity. As above, we make this comparison for all *actgrad* circuits extracted from the regularized model. Bias removal only has an effect at high sparsities (<.1), and that effect is usually small. Sometimes bias removal even has a positive effect, leading to a better feature-preserving circuit (dots above the red 0-line).

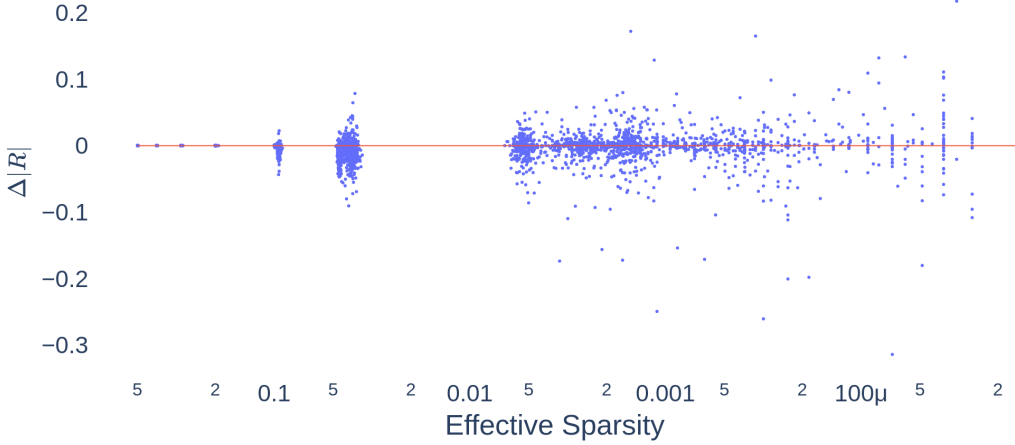


Figure 9: Circuit $\Delta|R|$ (Pruned - Masked)

6.3 Sparsity Regularizer

To obtain a regularized version of Alexnet with kernel-wise sparsity, we used hierarchical group sparse regularization Mitsuno *et al.* (2020), utilizing the associate code, <https://github.com/K-Mitsuno/hierarchical-group-sparse-regularization>. We utilized a combination of hierarchical squared group l1/2 regularization $R_{1/2}$ as well as simple L1 regularization R_1 . For a given convolutional layer's weight matrix \mathcal{W}_l , these regularization terms are defined as;

$$R_{1/2}(\mathcal{W}^l) = \sum_{j=1}^{C_{in}^l} \left(\sum_{i=1}^{C_{out}^l} \sqrt{\sum_{h=1}^{K_h^l} \sum_{w=1}^{K_w^l} |w_{i,j,h,w}^l|} \right)^2, \quad R_1(\mathcal{W}^l) = \sum_{j=1}^{C_{in}^l} \sum_{i=1}^{C_{out}^l} \sum_{h=1}^{K_h^l} \sum_{w=1}^{K_w^l} |w_{i,j,h,w}^l| \quad (16)$$

These regularization terms are then combined with the typical cross-entropy loss \mathcal{L}_{ce} to obtain the loss used to train the model;

$$\mathcal{L} = \mathcal{L}_{ce} + \lambda_2 \sum_{l=1}^L \lambda_1 R_{1/2}(\mathcal{W}^l) + (1 - \lambda_2) \sum_{l=1}^L \lambda_1 R_1(\mathcal{W}^l) \quad (17)$$

Where λ_1 scales the regularization terms, and λ_2 sets the balance between $R_{1/2}$ and R_1 . We used $\lambda_1 = .002$ and $\lambda_2 = .6$. We then finetuned a pretrained Alexnet model with this regularizer for 50 epochs using SGD, with a LR=.001, and momentum=.7. The resultant model achieves a top-1 accuracy of 53.03% on ImageNet, where the original model achieves 56.55%. From the first convolutional layer to last, the model has the following proportions of kernels *remaining*, as determined by ($\mathcal{S}_{magnitude} > .001$): 1.0, 0.820, 0.538, 0.634, 0.581.

6.4 FORCE scheduler

Following the original paper de Jorge *et al.* (2020), we used an exponential decay scheduler for determining the size of the mask at each iteration. Given an iteration t and m relevant kernels, the number of kernels masked k_t at t is given by;

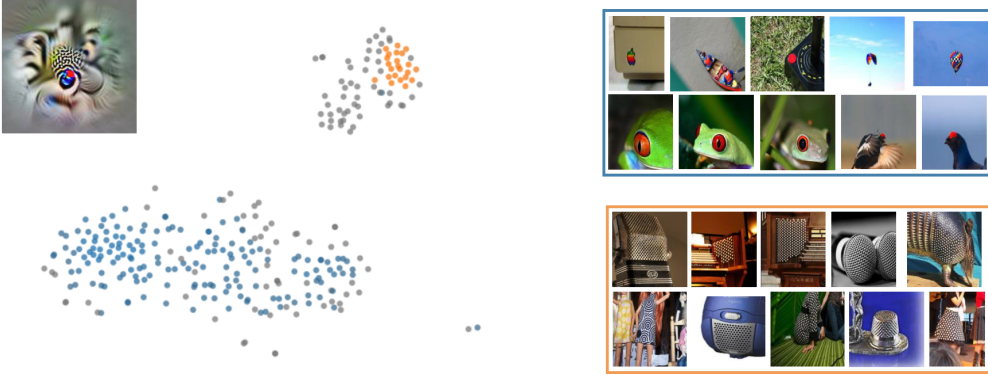
$$k_t = \exp\{\alpha \log k + (1 - \alpha) \log m\}, \quad \alpha = \frac{t}{T} \quad (18)$$

We used 10 iterations in our experiments ($T = 10$).

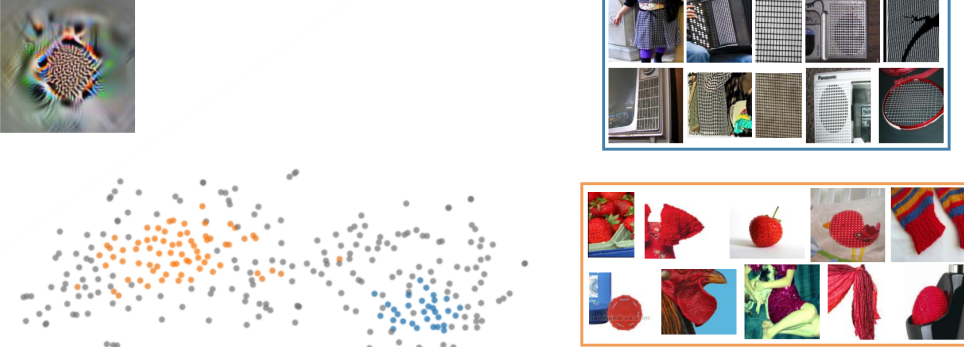
6.5 Clustering

Fig 10 shows some additional examples of *clusterable* features identified by our clustering analysis. For each feature we show a 2D t-SNE plot der Maaten & Hinton (2008) of the 300 population vectors, with clusterable points colored blue and orange. Sample image patches belonging to each cluster are shown on the right. Many of the clusters correspond to images of dogs, perhaps due to the preponderance of dog categories in Imagenet.

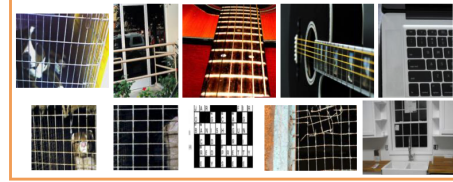
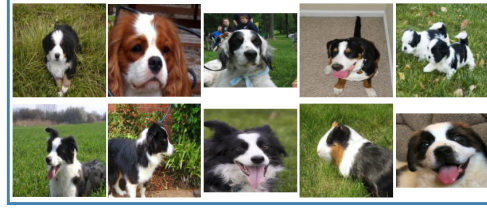
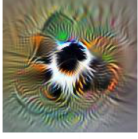
Conv4:39



Conv4:81



Conv5:148



Conv5:108



Figure 10: clusterable features, with TSNE projection

6.6 Conv4:53 Top activating image patches

Fig 11 shows a sample a top activating image patches for *Conv4:53*. These image patches motivated the big/small sub-feature circuit extraction experiment, as we hypothesized the feature was a scale invariant circle detector.

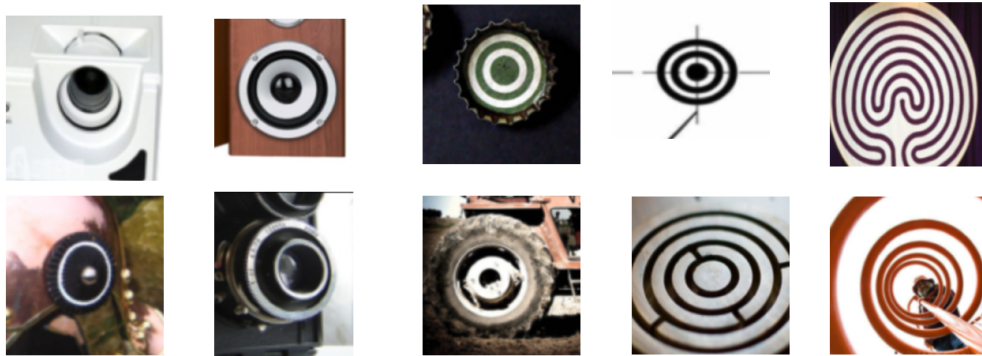


Figure 11: Sample activating image patches for *Conv4:53*

6.7 Circuit Diagram GUI

Our circuit diagramming tool has a GUI to aid circuit analysis. Individual vertices and edges can be isolated with the point and click interface, as shown in Fig 12. The interface also offers sliders for dynamically adjusting the size of displayed kernels and feature visualizations. The user can zoom in on any section of the diagram with a built in cropping tool. Hovering over graph components shows meta-data, like the feature ID of the component and its saliency score. The tool can be accessed through the provided notebook; github.com/chrishamblin7/circuit_pruner/circuit_diagram.ipynb

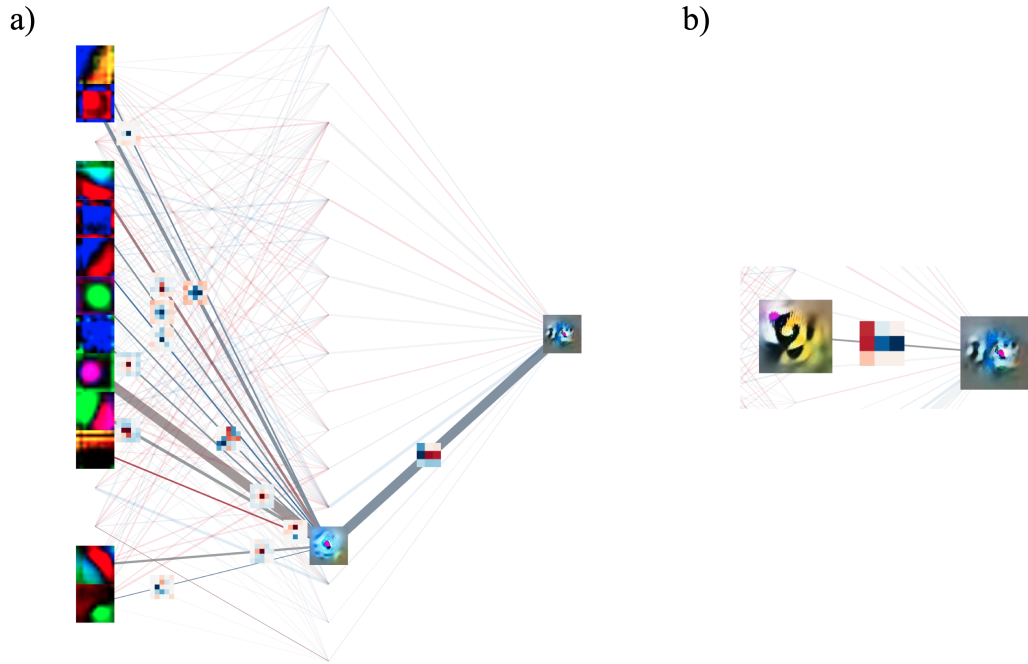


Figure 12: *a)* GUI vertex selection. *b)* GUI edge selection